Lunar laser ranging and the equivalence principle signal

Jürgen Müller*
Institute for Astronomical and Physical Geodesy, TU München, Arcisstrasse 21, D-80333 München, Germany

Kenneth Nordtvedt†
Northwest Analysis, Box 2139, Friday Harbor, Washington 98250
(Received 12 February 1998; published 10 August 1998)

The fitting of 28 years of lunar laser ranging data for a possible range signal indicating an equivalence principle-violating difference in the gravitational acceleration rate of Earth and the Moon toward the Sun is performed and then examined, both analytically and by computer simulations. The EP-violating signal is synodic, being predominately proportional to $\cos D$ (D is the synodic phase). Because LLR data do not uniformly sample the synodic month cycle, almost any hypothesis of a specific post-model synodic range signal responds strongly and with bias to the presence of most any other un-modeled synodic range effect. Since the physical and operational structure of the LLR experiment is of synodic periodicity, many of its modeling problems tend to be synodic: so we have created a synodic phase, bin-averaged presentation of the experiment's post-fit range residuals. By this technique the entire structure of the synodic modeling inadequacies can be detected without preconceptions or hypotheses as to their particular form. A synodic post-model residual signal of characteristic size 1 cm is found in the data. An observation "worth" function has been found which quantifies the potency of each additional observation for reducing the rms noise uncertainty in the fit of the $\cos D$ amplitude. It strongly indicates that LLR observations should, for some time into the future, preferentially be made on the new moon side of the quarter moon phase. [S0556-2821(98)06216-X]

PACS number(s): 04.80.Cc, 95.10.Ce, 95.30.Sf

I. INTRODUCTION

If Earth and Moon accelerate toward the Sun at different rates, the resulting perturbation of the Earth-Moon distance is [1]

$$\delta r_{em} \simeq A_{\mathrm{EP}} \cos D + \text{small harmonic and eccentric sidebands.} \quad (1)$$

D is the synodic lunar phase. The subscript EP stands for *equivalence principle*; the foundation for Einstein's equivalence principle is the apparent fact that all bodies accelerate at the same rate in gravity (neglecting tidal gradients). The proportionality of this range perturbation amplitude to the fractional difference δ_{em} in the acceleration rates of Earth and the Moon toward the Sun has recently been reevaluated both analytically and by computer methods [2,3] and is

$$A_{EP} \simeq 2.9 \times 10^{12} \delta_{em} \ \mathrm{cm} \quad (2)$$

with

$$\delta_{em} \equiv \left| \frac{\vec{a}_e - \vec{a}_m}{\vec{g}_s} \right|. \quad (3)$$

There is a Newtonian perturbation of the lunar orbit, due to the tidal gradient of the Sun's gravity, which also produces Earth-Moon range variations proportional to $\cos D$ (historically called the *parallactic inequality*), but the fixing of the gravity model parameters determines this Newtonian amplitude with uncertainty of less than a millimeter.

By fitting over 11 000 lunar laser ranging (LLR) measurements accumulated over the last 28 years to a detailed model for the Earth-Moon range, analysis groups now place what are called "realistic uncertainty" limits on the EP-violating amplitude of slightly more than a centimeter,

Williams *et al.* [4]

$$A_{EP} = -0.8 \ \mathrm{cm} \ \text{with "realistic uncertainty" } 1.3 \ \mathrm{cm}, \quad (4)$$

Müller *et al.* [5]

$$A_{EP} = +1.1 \ \mathrm{cm} \ \text{with "realistic uncertainty" } 1.1 \ \mathrm{cm}, \quad (5)$$

indicating near equality of acceleration rates of Earth and the Moon toward the Sun and "realistic uncertainty":

$$\delta_{em} \lesssim 4 \times 10^{-13}. \quad (6)$$

The almost 2 cm difference between these two recent values for A_{EP} is notable and is discussed further in our Conclusions section. For perspective on these fits, a 1 cm amplitude will be produced by a metric theory of gravity with parametrized post-Newtonian (PPN) coefficients $4\beta - 3 - \gamma \simeq 7 \times 10^{-4}$. General relativity yields a null value for this amplitude.

As remarkable as these fits are, the potential exists for measuring the amplitude $A_{EP} \equiv A_D$ to even higher precision. If N well distributed observations with rms measurement er-

*Email address: jxmx@alpha.fesg.tu-muenchen.de
†Email address: kennordtvedt@one800.net

rors σ are available to fit solely for such a signal amplitude, one can ideally achieve a formal rms estimation precision of

$$|\delta A_D| \simeq \sqrt{\frac{2}{N}}\,\sigma. \tag{7}$$

A rough estimate of this measurement ideal is made by considering the highest quality observations of the last decade: $N \simeq 5000$, $\sigma \simeq 4$ cm. This suggests a potential formal rms error of about .08 cm for the amplitude. In this paper we seek to better understand the reasons for the difference between the ideal formal precision and the "realistic" precision of the lunar laser ranging (LLR) fits for this amplitude, and then work toward modifications or additions to the experimental and analysis procedures so as to produce experimental fits closer to the formal limits of the data.

Much of this investigation is concerned with the consequences of a key property of the actual LLR data: the nonuniformity of the data density over the synodic phase. Ranging measurements are rare near new and full moon and cluster around quarter moon phases, and their occurrence is significantly biased toward a full moon. For a couple of reasons, this reduces the "realistic" precision which can be given to the measurement of the synodic signal amplitude A_D. First, and perhaps most importantly, this synodic modulation of the data density increases the tendency of other unmodeled synodic effects in the data to bias the estimation of the amplitude A_D, and second, it weakens the effective strength of the cos D signal by confining the fit to the vicinity of the quarter phase, and thereby increases the formal error for estimating its amplitude. The ease with which the presence of one synodic signal can bias the estimation of another in an actual fit of the LLR model has led us to construct and present synodic phase, bin-averaged post-fit residuals. Viewing the plots of these quantities facilitates perceiving the entire structure and quality of the fit (or misfit) of synodic effects, without preconceptions as to the shape and origins of any statistically significant structure in these bin-averaged post-fit residuals.

We find a synodically periodic post-fit residual signal in the Earth-Moon range of 1 cm characteristic size over the synodic phase range of about $40° < D < 150°$ (from the nearest new moon). The statistical significance of the post-fit residual averages nearer to new and full moons is presently negligible due to sparce data. The bin-averaged presentation of post-fit residuals can also be used for the various other periodicities of the LLR data which are related to testing different scientifically interesting range signals.

II. LLR MODEL

A brief overview is given of the procedure for fitting LLR data to a multi-parameter theoretical model (see also [6]). Details of this procedure touch on the ability to then test for the presence of scientifically interesting post-model signals such as the EP-violating signal previously mentioned. The LLR basic model (hereafter referred to as simply "the model") is the comprehensive theory which is used to predict, by computer-assisted calculation, the values of the LLR observables—the round trip times of flight of laser pulses between stations on Earth and passive reflectors on the Moon. The model contains a large number M of parameters whose values are not *a priori* known with sufficient precision to match the quality of the observations, and they are therefore best determined by using the LLR data. These parameters include the initial conditions (positions, velocities, orientations, etc.) of the key bodies such as Earth and the Moon, locations of laser stations and reflectors, body masses and gravitational multipole strengths, etc. A more specific description of the model is given in the Appendix. The model gives the N range observables as functions of the many model parameters and of the time (which also must be relativistically modeled):

$$O_i = O(P_m, t_i) \quad \text{with } m = 1 \text{ to } M,\ i = 1 \text{ to } N. \tag{8}$$

Small changes in the parameter values will then change the calculated values of the range observables by the small amounts

$$\delta O_i = \sum_{m=1}^{M} \frac{\partial O_i}{\partial P_m}\,\delta P_m. \tag{9}$$

For purposes of streamlining equations, we here switch to a vector notation by introducing N-dimensional vectors in *observation space*; the previous equation is then expressed as

$$\delta\vec{O} = \sum_{m=1}^{M} \vec{f}(m)\,\delta P_m \quad \text{with} \quad \vec{f}(m) \equiv \frac{\partial \vec{O}}{\partial P_m}. \tag{10}$$

Picking an initial set of values for the M parameters of the model, $P_m^{(0)}$, the initial residuals are then defined as the observed-minus-calculated values of the ranges

$$\vec{r} = \vec{O}(\text{obs}) - \vec{O}(P_m^{(0)}). \tag{11}$$

Optimally adjusted values for the model parameters

$$P_m^{(0)} \rightarrow P_m^{(0)} + \delta P_m \tag{12}$$

are then obtained by finding the weighted least-squares-fit of the residuals,

$$\text{minimize} \left(\vec{r} - \sum_m \vec{f}(m)\,\delta P_m\right) \cdot \left(\vec{r} - \sum_n \vec{f}(n)\,\delta P_n\right), \tag{13}$$

with the solution

$$\delta P_n = \sum_m [\vec{f}(n) \cdot \vec{f}(m)]^{-1} \vec{f}(m) \cdot \vec{r}. \tag{14}$$

The inverse of the $M \times M$ matrix formed by the scalar products of the parameter partial functions is indicated. Scalar products are defined with respect to a weighting matrix:

$$\vec{a} \cdot \vec{b} \equiv \sum_i W_{ij} a_i b_j. \tag{15}$$

The weighting matrix which minimizes the formal estimation uncertainties for the model parameters is the inverse of the matrix of expected values of observation error products:

$$W_{ij}=\langle \delta O_i \delta O_j \rangle^{-1}. \tag{16}$$

If the observation errors are uncorrelated, this weighting matrix is simply the diagonal matrix of reciprocal mean squared errors, and this is the working assumption in most analyses:

$$W_{ij}=\frac{1}{\sigma_i^2}\delta_{ij}. \tag{17}$$

The post-fit residual vector consists of what is left of the residuals after the parameter adjustments given in Eq. (13) are made:

$$\vec{r}^{\,*}=\vec{r}-\sum_{m,n=1}^{M}\vec{f}(n)[\vec{f}(n)\cdot\vec{f}(m)]^{-1}\vec{f}(m)\cdot\vec{r}$$

$$\equiv(\mathbf{1}-\mathbf{P}_M)\cdot\vec{r}. \tag{18}$$

Post-fit residuals are more fundamental than the initial residuals. The latter depend on the accidental initial choices of model parameter values. The former are invariant quantities reflecting real noise and inadequacies of the model. The projection operator $\mathbf{P}_M$ defined above establishes the model's M-dimensional subspace within the N-dimensional observation space of the experiment. This matrix operator consists of the sum of outer products of any set of M orthogonal unit vectors which span the sub-space of the model parameter's partial functions $\vec{f}(1)\cdots\vec{f}(M)$. This can be seen by considering the special case of orthogonal combinations of the parameter partial vectors, in which case

$$\mathbf{P}_M=\sum_{m=1}^{M}\frac{1}{\vec{f}(m)'\cdot\vec{f}(m)'}\vec{f}(m)'\vec{f}(m)'=\sum_{m=1}^{M}\hat{u}(m)\hat{u}(m). \tag{19}$$

Although this projection operator is a unique matrix object, it can be expressed by an unlimited number of representations, of which certain ones are particularly useful for its construction and use. Selecting any of the orderings of the M model parameters, a corresponding set of M orthogonal unit vectors defining the model's subspace is constructed by the sequential process

$$\hat{u}(1)=\frac{1}{[\vec{f}(1)\cdot\vec{f}(1)]^{1/2}}\vec{f}(1) \quad \text{then for} \quad m=2,\ldots,M \tag{20}$$

$$\vec{g}(m)=\vec{f}(m)-\sum_{m'=1}^{m-1}\hat{u}(m')\hat{u}(m')\cdot\vec{f}(m) \tag{21}$$

$$\hat{u}(m)=\frac{1}{[\vec{g}(m)\cdot\vec{g}(m)]^{1/2}}\vec{g}(m) \tag{22}$$

and then

$$\mathbf{P}_M=\sum_{m=1}^{M}\hat{u}(m)\hat{u}(m). \tag{23}$$

Consider a situation in which an extra signal $\vec{H}=H\vec{h}$ is added to the model as a post-model hypothesis. This might be done, for instance, in an attempt to explain unexpected and structured post-fit residuals. The post-model hypothesis vector will necessarily be composed of a part lying within the model subspace and a remainder which lies without:

$$\vec{h}\equiv\mathbf{P}_M\cdot\vec{h}+(\mathbf{1}-\mathbf{P}_M)\cdot\vec{h}\equiv\mathbf{P}_M\cdot\vec{h}+\vec{h}^{\,*}. \tag{24}$$

Only the latter part of the vector from this hypothesis, the part lying outside the model subspace, plays a role in estimating the hypothesis parameter; the least-squares-fit procedure gives

$$H=\frac{\vec{h}^{\,*}\cdot\vec{r}}{\vec{h}^{\,*}\cdot\vec{h}}. \tag{25}$$

(Note that when one takes a scalar product of two vectors which are orthogonalized to the model sub-space, it is unnecessary to orthogonalize both.) The part of the vector $\vec{h}$ lying within the model subspace readjusts the estimated values of the model's original M parameters. These readjustments may be improvements which eliminate biasing of the original estimates of the model parameters if the post-model hypothesis comes close to correcting the actual inadequacies in the model.

Think of the residual vector as composed of three parts: (1) a signal proportional to the actual form assumed in the post-model hypothesis, (2) a signal representing yet other unmodeled, perhaps unknown, features of the experiment, and (3) random noise

$$\vec{r}=H_0\vec{h}+\vec{x}+\vec{n} \tag{26}$$

with

$$\langle\vec{n}\rangle=0 \quad \text{and} \quad \langle n_i n_j\rangle=\sigma_i^2\delta_{ij}. \tag{27}$$

The estimate for the parameter H will then include (1) a true recovery of the actual parameter value in reality H_0, plus (2) a bias of this estimate due to the yet-unmodeled signal $\vec{x}$, and (3) a noise-induced error of zero expected value but finite variance,

$$\langle H\rangle=H_0+\frac{\vec{h}^{\,*}\cdot\vec{x}}{\vec{h}^{\,*}\cdot\vec{h}}, \tag{28}$$

and noise-induced variance:

$$\langle(H-\langle H\rangle)^2\rangle=\frac{1}{\vec{h}^{\,*}\cdot\vec{h}}. \tag{29}$$

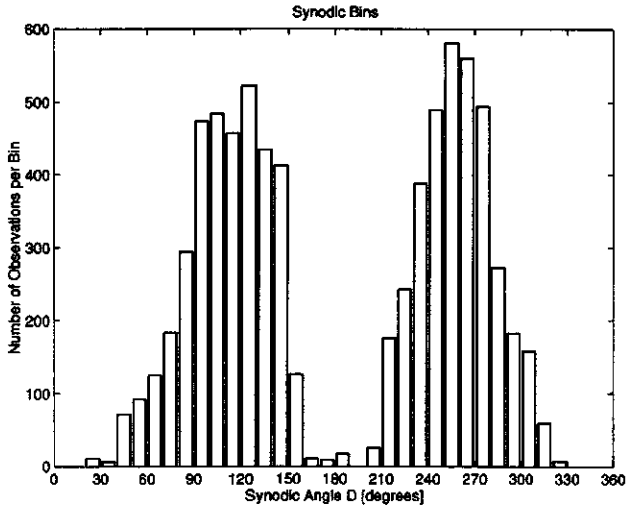

FIG. 1. Density of 1985–1997 LLR range data is shown as a function of synodic angle. The absence of data near new and full moons, and asymmetry of data density about quarter moon ($D=90$ and 270 degrees) weakens the quality of the fit for an equivalence principle violating signal.

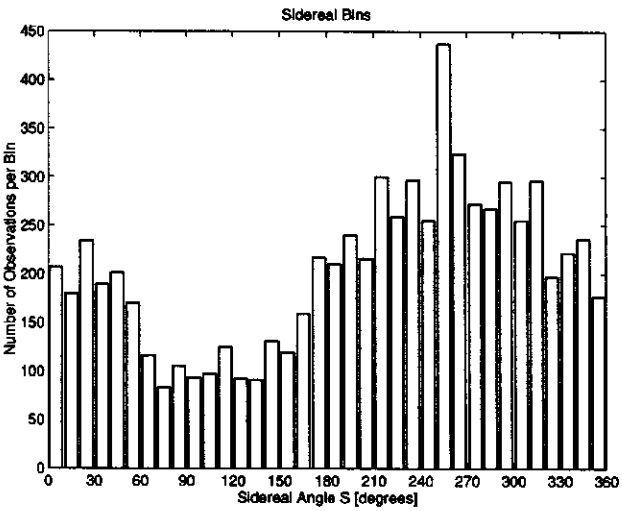

FIG. 2. Density of 1985–1997 LLR observations is shown as a function of sidereal angle, measured from the cosmic microwave radiation dipole asymmetry direction projected into the ecliptic plane. Observations are less frequent from the northern hemisphere laser stations when the Moon is in the southern sky. These sidereal data density modulations can mix annual effects with synodic effects in the analysis.

The "realistic uncertainties" in estimating hypothesis parameters found in the literature result from attempts to take into account both the noise errors and bias errors of this example.

III. DATA DENSITY MODULATIONS AND THEIR CONSEQUENCES

Because of operational realities, such as the difficulty to target laser reflector stations on the Moon when they are in darkness or excessive background solar illumination noise near new and full moons, LLR data have become concentrated near quarter moon synodic phases and are sparce as new and full moon phases are approached, though favoring the full moon side of the quarter moon phase. A distributional plot over the synodic phase of the 7364 LLR observations between 1985 and early 1997 is presented in Fig. 1. A Fourier representation of this data density distribution,

$$n(D)=n_0\left(1+\sum_n\left[C_n\cos(nD)+S_n\sin(nD)\right]\right), \quad (30)$$

yields the Fourier coefficient values

$$C_1\simeq-.50,\ C_2\simeq-1.09,\ C_3\simeq.61,$$
$$S_1\simeq.01,\ S_2\simeq-.20,\ S_3\simeq.25. \quad (31)$$

The coefficient C_2 quantifies the rarity of observations near new and full moons, while the coefficients C_1 and C_3 indicate asymmetry about a quarter moon and S_2 and S_3 asymmetry about a new moon. If the data distribution were uniform across the synodic phase, the various synodic harmonic signals would be quasi-orthogonal, but now they substantially project onto each other and acquire altered norms. Some typical scalar products among such signals are

$$\sum_i \cos D_i\cos 2D_i\simeq\frac{n_0T}{4}(C_1+C_3) \quad (32)$$

$$\sum_i t_i\cos D_i\sin 2D_i\simeq\frac{n_0T^2}{8}(S_1+S_3) \quad (33)$$

$$\sum_i \cos D_i\simeq\frac{n_0T}{2}C_1 \quad (34)$$

$$\sum_i \cos^2 D_i\simeq\frac{n_0T}{2}\left(1+\frac{1}{2}C_2\right). \quad (35)$$

These properties have major consequences for understanding outcomes of LLR data analysis and play an important role throughout the rest of this paper.

There is also substantial sidereal modulation of the data density as seen in Fig. 2. This results from the shorter time periods available from laser observatories in the northern hemisphere (Grasse, France; Haleakala, Hawaii; McDonald Observatory, Texas) for good observation of the Moon when it is in Earth's southern hemisphere sky (which occurs with sidereal period). By contrast, annual and lunar anomalistic (perigee to perigee) modulations of the data density are found to be minimal.

IV. EQUIVALENCE PRINCIPLE VIOLATION SIGNAL

A most significant scientific effect which is sought in the LLR data is the previously mentioned synodic cos D signal with amplitude proportional to any difference in the acceleration of Earth and the Moon toward the Sun. This could

occur if the Sun's gravity couples in a non-universal way to the Earth's and Moon's various forms of energy content—nuclear, electromagnetic, weak, gravitational [7]—or if part of the coupling is in proportion to some other attributes of the participating bodies. All of these cases would require a modification of gravitational theory and/or the addition of new long-range interaction fields to physical law. If such a post-model signal is hypothesized (the model assumes general relativity theory),

$$H(D)=A_D \cos D, \tag{36}$$

then the formal precision with which the amplitude of this hypothesis can be measured is obtained by application of Eq. (29):

$$\delta A_D=\frac{1}{\sqrt{\langle \cos D|\cos D^*\rangle}}. \tag{37}$$

The shorthand notation of Dirac is here adopted for expressing vector scalar products in the N-dimensional observation space. And one is reminded that the asterisk on a vector indicates that the vector has been orthogonalized to the model's M-dimensional subspace.

As previously mentioned, construction of the model's projection operator can be done by using any convenient ordering of the model's M partial vectors. For our purposes of studying synodic signals, we choose the first two model partials to be those which project strongest into the space of synodically periodic signals such as the EP-violating signal. These partials are those of the model parameters: (1) the mean distance of the laser reflectors from Earth and (2) the Newtonian gravitational mass parameter GM_{e+m} of Earth plus Moon. The dominant synodic parts of these partial vectors are

$$\tilde{f}(1)_i \simeq 1, \quad \tilde{f}(2)_i \simeq \cos 2D_i. \tag{38}$$

For brevity we denote these vectors $|0\rangle$ and $|2D\rangle$, respectively. Applying the procedure for constructing orthonormal unit vectors of the model as outlined in Eqs. (20)–(22), we obtain

$$\hat{u}(0)=\frac{1}{\sqrt{\langle 0|0\rangle}}|0\rangle \tag{39}$$

$$|2D^*\rangle=|2D\rangle-\frac{\langle 0|2D\rangle}{\langle 0|0\rangle}|0\rangle. \tag{40}$$

These vectors then are used to orthogonalize the vector $|\cos D\rangle \equiv |D\rangle$ from the model:

$$|D^*\rangle=|D\rangle-\frac{\langle 0|D\rangle}{\langle 0|0\rangle}|0\rangle-\frac{\langle D|2D^*\rangle}{\langle 2D|2D^*\rangle}|2D^*\rangle. \tag{41}$$

The analytic estimate of the formal error for estimating A_D, using Eq. (37) and the projections from Sec. III which result from the synodic variations of the data density, is then

$$\delta A_D \simeq \sqrt{\frac{2}{N}}\,\sigma\sqrt{\frac{2}{2+C_2-C_1^2-(C_1+C_3-C_1C_2)^2/(2-C_2^2)}} \simeq .15 \text{ cm} \tag{42}$$

which should be compared with the ideal estimate given in Eq. (7). The synodic modulations of the data density have almost doubled the formal error in estimating this amplitude. The actual formal error for the A_D amplitude is found to be 0.19 cm.

The post-fit residual signal which results from various unit cos(nD) residual signals can also be analytically approximated using the results from Eqs. (39) and (40) and Sec. III. We find strong distortion of these signals,

$$|nD^*\rangle \cong |nD\rangle-\frac{1}{2}C_n|0\rangle - \frac{C_{|n-2|}+C_{n+2}-C_2C_n}{2-C_2^2}\left(|2D\rangle-\frac{1}{2}C_2|0\rangle\right), \tag{43}$$

which, for $n=1,2,\ldots,$

$$\cong |D\rangle+.54|0\rangle+.53|2D\rangle \tag{44}$$

$$\cong 0 \text{ because } |2D\rangle \text{ is close to one of the model signals} \tag{45}$$

$$\cong |3D\rangle-.42|0\rangle-.21|2D\rangle \tag{46}$$

$$\cong |4D\rangle+.73|0\rangle+1.34|2D\rangle \tag{47}$$

$$\cong |5D\rangle-.41|0\rangle-.76|2D\rangle \ldots. \tag{48}$$

The analytically estimated post-fit residual signal $|D^*\rangle$ from this list is plotted in Fig. 3 along with the actual post-fit signal. The latter is obtained by a computer simulation process in which a unit cos D signal is added to the actual LLR range data, a new-least-squares-fit of the model is made, and the changes in the post-fit residuals are noted. This actual post-fit residual signal resulting from a unit cos D residual

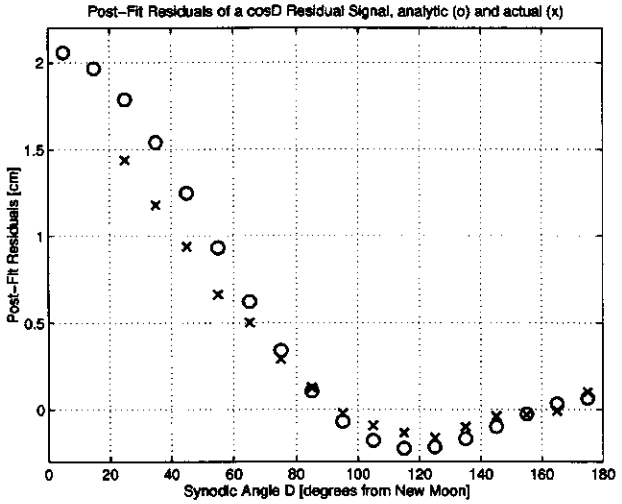

FIG. 3. The post-fit residuals signal resulting from a unit cos D signal in the residuals is determined both in analytical approximation and by actual computer simulation. The asymmetry of this post-fit signal is a result of the asymmetry of the experiment's accumulated data density about a quarter moon.

signal is also included in various other plots to serve as a calibrator for comparison with actual post-fit results.

The square of the components of this post-fit residual signal $|D^*\rangle$ as a function of synodic angle D has additional interesting significance. Since LLR is an ongoing experiment, it is useful to know the relative value of different additional observations in reducing the formal noise error in the estimation of the cos D amplitude. Noting from Eq. (37) that this rms uncertainty is the minus one-half the power of the norm of the post-fit signal, *after orthogonalization from the model*, we find that the reduction in $\delta A(D)_{rms}$ from an additional observation made at synodic phase D is (in arbitrary units)

$$\text{new moon}\quad D=00^\circ\ \delta A(D)_{rms}\sim -4.32 \tag{49}$$

$$D=30^\circ\sim -2.81 \tag{50}$$

$$D=60^\circ\sim -0.60 \tag{51}$$

$$\text{quarter moon}\quad D=90^\circ\sim -0.00 \tag{52}$$

$$D=120^\circ\sim -0.05 \tag{53}$$

$$D=150^\circ\sim -0.00 \tag{54}$$

$$\text{full moon}\quad D=180^\circ\sim -0.01. \tag{55}$$

As balance is restored between the total data on the two sides of the quarter moon phase by implementing the actions indicated by this "worth" function, the numerical coefficients (.54, .53) in Eq. (44) will tend toward zero, and the naive "worth" function $-\cos^2 D$ will be approached. In fundamental respects, the asymmetry of the data density about the quarter moon phase has become a more detrimental feature of the data set than the sparcity of data near new and full moons. But fortunately, this asymmetry is correctable by a selective schedule of future observations.

The formal precision for measuring the synodic amplitude A_D is only part of the basis for the published "realistic uncertainties" of over 1 cm. These conservatively stated precisions are not so much a measure of noise errors (though some arrive at their "realistic uncertainties" by using a heuristic multiplier of their formal uncertainties): they are rather the result of the generous allowance deemed necessary by analysts for possible systematic errors and inadequate modeling of the experiment. Improving the scientific product from the LLR data depends on reducing these modeling errors or omissions, but a first step must be to obtain clues about the structure of these modeling inadequacies.

Because of synodic modulations of the data density as shown in Fig. 1, the presence of almost any synodically periodic residual signal $R(D)$ will lead to a biased estimate of the EP-violating signal amplitude when this latter signal is hypothesized in isolation. If we fit the hypothesis

$$H(D)=A_D\cos D \tag{56}$$

the estimate of the amplitude is

$$A_D=\frac{\langle R(D)|\cos D^*\rangle}{\langle\cos D|\cos D^*\rangle}. \tag{57}$$

For various possible unit amplitude residual signals $R(D)=\cos(nD)$ we have analytically approximated the biased estimates which will occur for this simple hypothesis:

$$\text{bias in } A_D\cong\frac{\langle\cos D|\cos(nD)^*\rangle}{\langle\cos D|\cos D^*\rangle}\quad \text{for } n=3,4,5,6,\ldots \tag{58}$$

$$\cong\frac{(2-C_2^2)(C_{n-1}C_{n+1}-C_1C_n)-(C_1+C_3-C_1C_2)(C_{n-2}C_{n+2}-C_2C_n)}{(2-C_2^2)(2+C_2-C_1^2)-(C_1+C_3-C_1C_2)^2} \tag{59}$$

$$\cong -1.60\quad \text{from } R(D)=\cos 3D \tag{60}$$

$$\cong +0.09\quad \text{from } R(D)=\cos 4D \tag{61}$$

$$\cong +0.75\quad \text{from } R(D)=\cos 5D \tag{62}$$

$$\cong +0.00 \quad \text{from } R(D)=\cos 6D. \tag{63}$$

The actual biased estimates of A_D resulting from these residuals $R(D)=\cos(nD)$ are obtained from the computer simulation procedure described previously, and they are found to be -1.78, 0.30, 0.95, and $-.023$, respectively, in fair agreement with the analytical approximations. If there is then a synodically periodic residual signal in the LLR data resulting from incomplete modeling of the experiment, only limited significance can be given to testing the simple hypothesis which represents an EP-violating signal. A biased (false) estimate for that EP-violating amplitude will result from almost any other synodic effect.

One can try to improve the estimation process by enlarging the post-model hypothesis to include both a $\cos D$ and a $\cos 3D$ signal

$$H(D)'=A'_D \cos D+A'_{3D} \cos 3D. \tag{64}$$

(A $\cos 2D$ signal is not here considered in the post-model hypothesis because such a signal is about equal to the partial vector for one of the model's parameters. However, this is not exactly the case, and this possibility is considered in the Conclusions section of this paper.) The analytical fit for this two-amplitude hypothesis given by Eq. (64) results from the coupled equations

$$\begin{pmatrix} \langle D|D^*\rangle & \langle D|3D^*\rangle \\ \langle 3D|D^*\rangle & \langle 3D|3D^*\rangle \end{pmatrix}\begin{pmatrix} A'_D \\ A'_{3D} \end{pmatrix}=\begin{pmatrix} \langle r|D^*\rangle \\ \langle r|3D^*\rangle \end{pmatrix}. \tag{65}$$

Although the estimated amplitude of the $\cos D$ signal in this solution is not now biased by the presence of any $\cos 3D$ signal in the actual residuals, the estimate of both amplitudes of this hypothesis will still be biased by the presence of any higher synodic Fourier components in the residuals. This route of expanding the hypothesis to include ever-higher Fourier terms can be continued.

But finding that the synodic modulations of the data density make it difficult to make an unbiased estimate of any particular synodic signal in the presence of other unknown synodic signals in the residuals, we have developed a procedure in which bin-averaged post-fit residuals are formed as a function of synodic phase. This permits a global viewing of the entire synodically periodic post-fit residual signal, without preconceptions as to its particular shape or physical origin(s). Such a procedure is better matched to what, in fact, we believe is the present chief task for LLR analysis: mapping out the complete structure of the unmodeled synodic (and related) signals in the range data.

V. BIN-AVERAGED RESIDUALS

To enhance the visualization of the total structure in the post-fit residuals, having one of the periodicities in the Sun-Earth-Moon system dynamics or in the operational procedures of the experiment, it is useful to construct bin averages of the post-fit range residuals. For annual phase, or lunar sidereal, synodic or anomalistic phases, etc., the 360° phase range is divided into B bins of width $360°/B$. The weighted average of the residuals in each bin are constructed,

$$r(b)^*=\left(\sum_{i(b)} 1/\sigma_i^2\right)^{-1}\sum_{i(b)} r_i^*/\sigma_i^2 \quad \text{for each } b=1,\ldots,B \tag{66}$$

with the sum over $i(b)$ including all observations with the appropriate phase angle lying between $360°(b-1)/B$ and $360°b/B$. Our bins will typically be 10° wide ($B=36$). The weighting factor σ_i quantities are provided by the observers as range "normal point" uncertainties and include effects due to the finite laser pulse width, number of observed photons composing the normal point, short term noise fluctuations in the system electronics or in the atmospheric propagation delays, etc. Experimental noise which only varies significantly on time scales longer than the time span of normal point construction is not included in these weights.

The bin-averaged residuals acquire smaller noise-induced uncertainties by the averaging over the large number of individual range normal points contained in most of the bins:

$$\frac{1}{\sigma(b)^2}\cong\sum_{i(b)} \frac{1}{\sigma_i^2}. \tag{67}$$

This particular bin weighted average definition also permits a useful reexpression of Eq. (25) for estimating a post-model parameter whose corresponding partial function $\vec{h}$ is periodic. Constructing bins defined with respect to the appropriate periodicity, Eq. (25) takes the form of a sum over bins of bin-defined attributes,

$$H=\left(\sum_b [h(b)^*]^2/\sigma(b)^2\right)^{-1}\sum_b h(b)^* r(b)^*/\sigma(b)^2, \tag{68}$$

which can conveniently be used both visually and quantitatively in conjunction with the plots of bin-averaged residuals.

Another virtue of these bin-averages defined for a particular periodicity is that a residual signal having a different periodicity will be suppressed. Contributions from other residual signals will average out to near zero when (1) many cycles are present in the LLR data, (2) the periodicities are well sampled across phase, and (3) the two frequencies differ by a modest amount. For example, a unit amplitude signal of frequency ω' will affect bin averages defined for frequency ω, with experiment time span T, by an amount

$$\delta r(\omega)\sim\frac{\sin[(\omega-\omega')T/2]}{(\omega-\omega')T/2}. \tag{69}$$

The bin-averaged post-fit residuals of the LLR data are shown in Figs. 4–8, constructed for several system dynami-

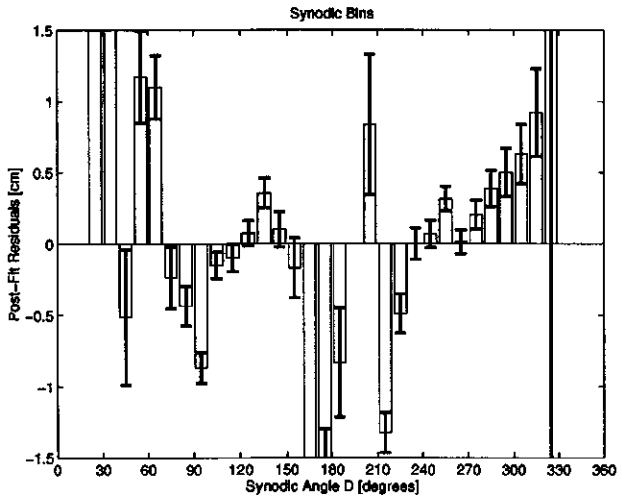

FIG. 4. Thirty-six bin weighted averages of the post-fit range residuals are shown as function of synodic phase. All observations during 1985–1997 which fall within each 10° interval of synodic phase (see Fig. 1.) contribute to the bin average. Bin error bars are composed only from the observer-supplied normal point errors.

cal frequencies of interest: synodic (D), sidereal (S), annual (Y), anomalistic (L), and "*meaningless*" (X) (chosen to be $\pi/4\times$ the synodic phase). The bars shown in these plots represent the formal noise errors for each bin average as computed from Eq. (67).

To obtain even better statistics for reducing noise errors, we plot in Fig. 9 weighted averages of the bins combined symmetrically about a new moon. This plot also shows the post-fit residuals signal (indicated by $\times$'s) which would result from a unit cos D signal in the residuals.

The plot of the "meaningles" phase was performed to see what magnitude of noise fluctuations would exist in bin averages for a phase which should have no connection with areal signal in the dynamics of the Sun-Earth-Moon system. This plot, along with that for the lunar anomalistic phase,

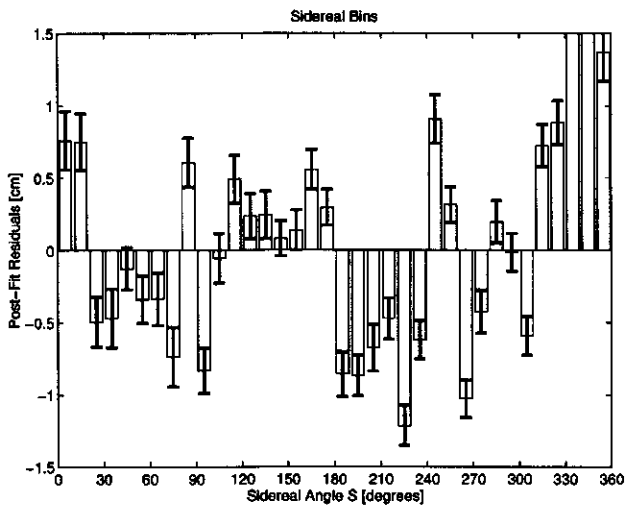

FIG. 5. Bin weighted averages of the post-fit range residuals are shown as function of the lunar sidereal phase.

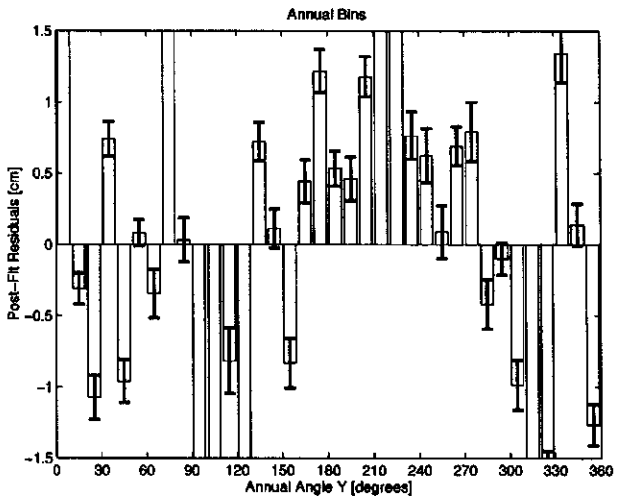

FIG. 6. Bin weighted averages of the post-fit residuals are shown as function of the annual phase, measured, like the sidereal phase, from the cosmic microwave radiation dipole asymmetry direction projected onto the ecliptic plane.

indicates that there is noise of a characteristic time scale longer than the time periods needed to construct the typical range normal point, and which therefore does not show up in the noise or uncertainty values supplied by the observers. But for purposes of using the entire collection of LLR data to fit the model, this extra noise is relevant to the correct estimation of the noise uncertainties in the parameter fits. Our estimate is that this inter-normal point noise about doubles the effective rms noise level from the observer-supplied values.

It is common for residual signals to be proportional to powers of both time and periodic signals. This occurs, for example, when frequencies or their time rates of change are initially mismodeled. If the synodic post-fit residuals are proportional to the combination

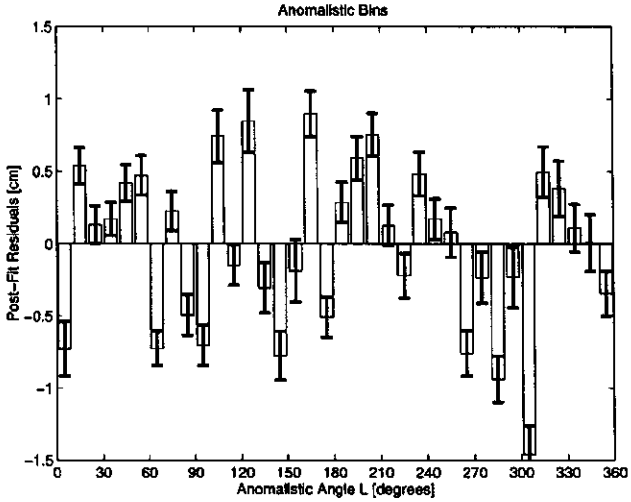

FIG. 7. Bin weighted averages of the post-fit residuals are shown as function of the lunar anomalistic (perigee to perigee) phase.

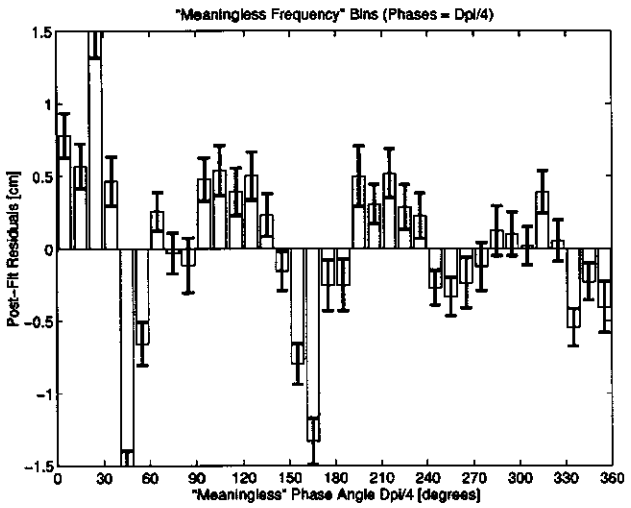

FIG. 8. Bin weighted averages of the post-fit residuals are shown as function of a "meaningless" phase ($\pi/4$ times synodic phase). This plot is performed to assess the size of additional noise fluctuations not captured in the observer-supplied normal point errors.

$$r(D,t)^* = f(D) + (t/T)g(D) \tag{70}$$

in which $f(D)$ and $g(D)$ are synodically periodic, t is the time of observation, and T is the total time of the data set, then bin averages can be defined which isolate the two synodically periodic functions:

$$f(D)_b = \frac{1}{S_0 S_2 - S_1^2} \sum_{i(b)} (S_2 - S_1 t_i/T) r_i^*/\sigma_i^2 \tag{71}$$

$$g(D)_b = \frac{1}{S_0 S_2 - S_1^2} \sum_{i(b)} (S_0 t_i/T - S_1) r_i^*/\sigma_i^2 \tag{72}$$

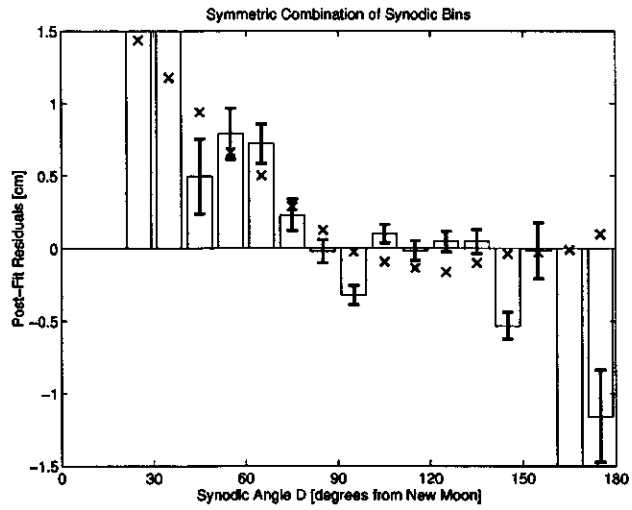

FIG. 9. For purposes of reducing noise fluctuations and improving the ability to see any cos D signal, we combine the data from bins D and $360° - D$ into 18 bins. The post-fit residual signal which will result from a unit cos D residual signal is also indicated.

with

$$S_n = \sum_{i(b)} (t_i/T)^n/\sigma_i^2. \tag{73}$$

We have not here produced these separated bin averages for the synodic post-fit residuals because theoretical considerations conclude that the $g(D)$ function should be antisymmetric about a new moon (proportional to the Fourier component sin $2D$), and therefore not strongly interfere with the structure of the even synodic function. However, a deeper analysis of the data using this separation procedure should be made.

VI. CONCLUSIONS

The result given in Eqs. (4) and (5), that there is an almost 2 cm difference between the recent fits for the EP-violating parameter A_D made by two analyst groups, requires comment. This difference cannot be due to the true noise in the LLR data. Since both results depend on almost the same range data, they are subject to the same set of noise values in the observations, and this will produce almost equal noise errors in the two estimated values for A_D. There must be some significant difference between the two models used for the fits to produce such different values for A_D. It is important to find these differences.

We have fit the LLR data with a sequence of increasingly complex hypotheses, beginning with the basic model alone, and then the model plus the post-model synodic signals:

$$H(D) = A_D \cos D \tag{74}$$

$$H(D)' = A_D' \cos D + A_{3D}' \cos 3D \tag{75}$$

$$H(D)'' = A_D'' \cos D + \sum_{n=3}^{7} A_{nD}'' \cos(nD). \tag{76}$$

For the model alone we obtained the estimated value for the Earth-Moon mass parameter [all $\pm$ values below are the formal $(1-\sigma)$ uncertainties based only on the observer-supplied normal point uncertainties; we find there to be additional noise between the normal points]:

$$GM_{e+m}^{(0)} = 403\,503.2415 \pm .0004 \ \text{km}^3/\text{s}^2 \tag{77}$$

expressed in TDB (barycentric dynamical time) units. For the three fits which included the successive post-model hypotheses we obtained

$$GM_{e+m} = 403\,503.23937 \pm .00055 \ \text{km}^3/\text{s}^2 \tag{78}$$

$$A_D = 1.15 \pm 0.19 \ \text{cm} \tag{79}$$

$$GM_{e+m}' = 403\,503.23697 \pm .00068 \ \text{km}^3/\text{s}^2 \tag{80}$$

$$A_D' = 2.68 \pm 0.32 \ \text{cm} \tag{81}$$

$$A_{3D}' = 0.85 \pm 0.14 \ \text{cm} \tag{82}$$

$$GM''_{e+m}=403\ 503.23492\pm.00108\ \text{km}^3/\text{s}^2 \tag{83}$$

$$A''_D=3.32\pm0.40\ \text{cm} \tag{84}$$

$$A''_{3D}=1.64\pm0.30\ \text{cm} \tag{85}$$

$$A''_{4D}=0.77\pm0.24\ \text{cm} \tag{86}$$

$$A''_{5D}=0.80\pm0.25\ \text{cm} \tag{87}$$

$$A''_{6D}=0.51\pm0.17\ \text{cm} \tag{88}$$

$$A''_{7D}=0.13\pm0.13\ \text{cm}. \tag{89}$$

Suspecting that a pure $\cos 2D$ signal may weakly separate from the partial signal for the Earth-Moon mass parameter, rendering its amplitude measurable, we also fitted the post-model hypothesis

$$H(D)'''=A'''_D\cos D+A'''_{2D}\cos 2D \tag{90}$$

and obtained

$$GM'''_{e+m}=403\ 503.2353\pm.0012\ \text{km}^3/\text{s}^2 \tag{91}$$

$$A'''_D=1.07\pm0.19\ \text{cm} \tag{92}$$

$$A'''_{2D}=-1.29\pm0.31\ \text{cm}. \tag{93}$$

The estimates of the amplitudes in the two-parameter fit given by Eqs. (81) and (82) are actually highly correlated, and a better way to express those values is

$$R(D)_{\text{est}}=(-.12\pm.07)(\cos 3D-.37\cos D) \tag{94}$$

$$+(2.63\pm30)(\cos D+.37\cos 3D)\ \text{cm}. \tag{95}$$

Actually, all multi-parameter solutions consist of a least-squares-fit "point" in multi-parameter space, plus a surrounding formal error ellipsoid. The axes of the error ellipsoid do not in general align themselves with the parameter axes, and the length of the different ellipsoid axes may vary greatly among themselves, indicating that certain parameter combinations are estimated with much higher precision than others.

The larger formal errors of the $\cos 2D$ amplitude and the Earth-Moon mass parameter given by Eqs. (91) and (93) reflect the high correlation (about 0.9) of those parameters' partial vectors. Comparing this fit with the basic model estimate in Eq. (77), the high sensitivity of the Earth-Moon mass parameter estimate to the presence and nature of other synodically periodic post-model hypotheses is noted. This reflects the ease with which the presence of any unmodeled synodic signal will bias that basic model parameter, suggesting that it may become preferable to use a fixed value for this mass parameter which can be obtained from a combination of laser ranging to satellites, from Viking ranging data which measures the Earth/Moon mass ratio, and from the Clementine and other future missions which directly mapped out the Moon's gravitational field. This model change would significantly increase the precision for measuring the EP-violating amplitude A_D. The realistic error associated with such a mass parameter is about .0025 km^3/s^2 which is equivalent to about 0.6 cm uncertainty in the $\cos 2D$ amplitude in the Moon's motion. So our exploratory fit given by Eqs. (91)–(93) indicates some significant unmodeled $\cos 2D$ signal which is accompanying the rest of the unmodeled synodic signal we are finding in the fits of Eqs. (78)–(89). At this time we view the chief goal of LLR data analysis to be the discovery of the detailed shape of the total unmodeled synodic range signal without preconceptions as to its origins, and by this approach to acquire clues as to what are the particular inadequacies in the model.

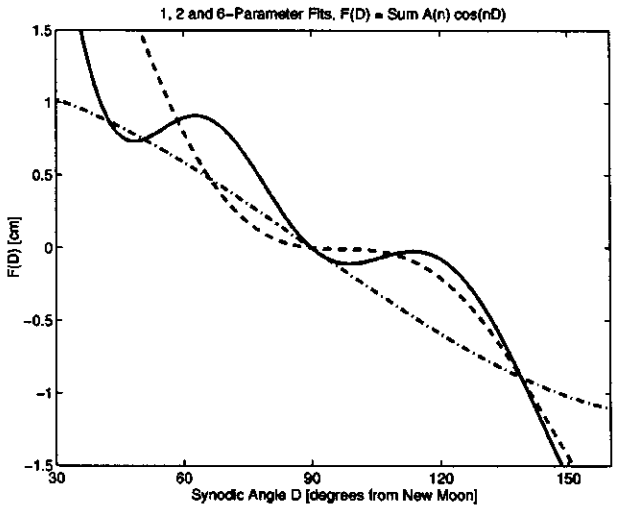

FIG. 10. The one-, two-, and six-parameter post-model fits [Eqs. (78)–(89)] for synodic residuals in the LLR observations are compared in one plot. An unknown amount of $A+B\cos 2D$ could also be present in the unmodeled range signal, but that signal would mostly be absorbed by adjustment (bias) of the model parameters. These three fits are consistent within the noise fluctuations of the data over the range of synodic angle of $40°<D<150°$ for which a plentiful quantity of data exists.

The three fits for the unmodeled range signal presented in Eqs. (78)–(89) are plotted in Fig. 10, including differences in the amplitude of a $\cos 2D$ contribution which are implied by the differences in the obtained values of the Earth-Moon mass parameter which accompanied each fit. [There is still a common but unknown amount of a $\cos 2D$ contribution to all three of the curves which is not included, though the fit given in Eqs. (91)–(93) suggests the size of this common amplitude.)

The three fits are rather consistent with each other in representing the unmodeled synodic signal over the range $40°<D<150°$ for which a good quantity and quality LLR data have been collected. These curves begin to seriously diverge as the new and full moon phases are approached, but that is where the data are sparce and the fits naturally have less significance. The robust information which has been discovered concerning the unmodeled synodic residual signal is that it includes a sloping line or curve which decreases by

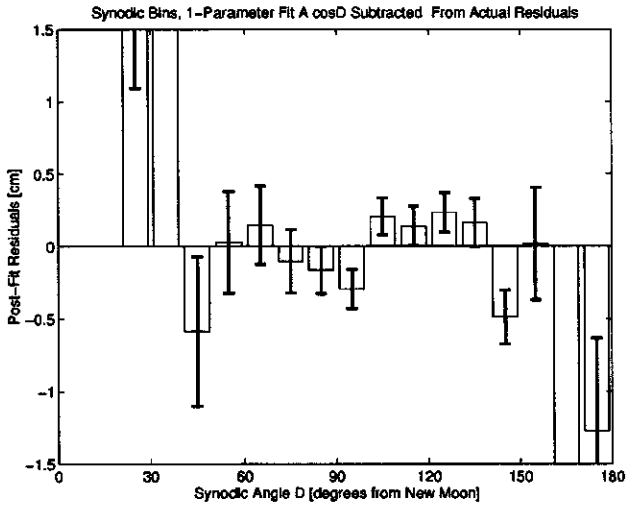

FIG. 11. The fit of the one-parameter hypothesis $A_D \cos D$ was subtracted from the actual LLR residual data, and the synodic bin-averaged post-fit residuals reobtained and here plotted. The error bars are doubled from the observer-supplied normal point errors, reflecting our determination that additional noise error between normal points exists.

about 2 cm over the interval of synodic angle of $40° < D < 150°$. Further details of the actual signal cannot be reliably specified with the present data.

We constructed "corrected" synodic phase bin-averaged post-fit residuals by subtracting either the one-parameter hypothesis fit given by Eq. (79) or the two-parameter hypothesis fit given by Eqs. (81) and (82) from the actual LLR data, obtaining a new model fit and bin-averaged post-fit residuals in each case. The results are plotted in Figs. 11 and 12. The bin-average error bars used in these plots have been doubled from the formal errors shown in the original synodic plot of Fig. 5. This was done because of our discovery that there apparently is inter-normal-point noise which is not captured

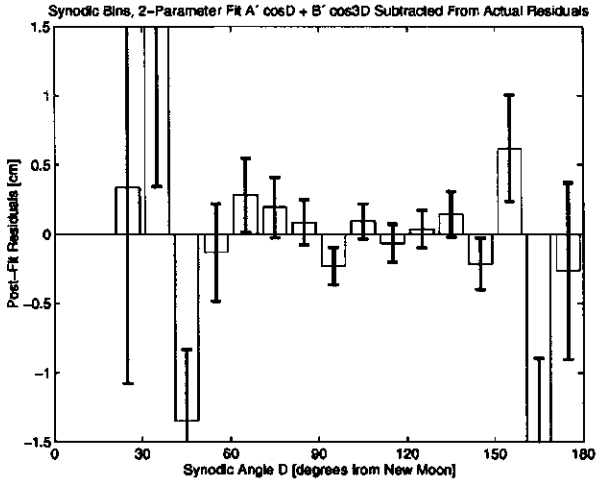

FIG. 12. The fit of the two-parameter hypothesis $A'_D \cos D + A'_{3D} \cos 3D$ was subtracted from the actual LLR residual data, and the synodic bin-averaged post-fit residuals reobtained and here plotted. Error bars are doubled from the supplied normal point errors.

in the noise internal to a normal point and estimated by the observers. We estimate that this consideration about doubles the actual data noise.

The most evident inadequacy in the model which we have identified concerns the tidal displacements of laser station positions on Earth and reflector positions on the Moon. The model presently computes these quantities under the idealization that Earth and the Moon tidally distort as fluid bodies characterized by constant vertical and horizontal *Love* numbers:

$$\delta\vec{r} = \frac{m^* a^4}{2mR^3}\{H_2[3(\hat{R}\cdot\hat{a})^2 - 1]\hat{a} + 6L_2\hat{R}\cdot\hat{a}(\hat{R} - \hat{R}\cdot\hat{a}\hat{a})\} \tag{96}$$

m and a are the mass and radius of the bodies being tidally distorted, and m^* and R are the mass and distance of the bodies producing the tidal distortions. The unit vectors point toward the appropriate sites and bodies, while H_2 and L_2 are the geophysical quadrupolar Love numbers for vertical and horizontal displacement. The model uses the nominal values recommended by the IERS Conventions: $H_2 = .6026$ and $L_2 = .0831$. On Earth

$$\frac{m^* a^4}{2mR^3} \simeq 18 \text{ cm and } 8 \text{ cm for lunar and solar tides, respectively.} \tag{97}$$

The Moon's next order octupolar tide on Earth is smaller by the factor $a/R \sim 1/60$ and has the characteristic size of a few millimeters. It is not presently included in the model, but we added it as a post-model correction and found it changed the synodic post-fit residuals by at most a small fraction of a millimeter over the range of the synodic phase, $40° < D < 150°$.

We tested the simplified tidal model by letting the Love numbers for the laser stations be independent, to-be-fit-for parameters in the model. We found statistically significant changes from the nominal values for the two stations which have supplied the bulk of the LLR data, Grasse, France and McDonald Observatory in Texas:

$$\delta H_2(G) = +.036 \pm .011, \quad \delta L_2(G) = +.040 \pm .004 \tag{98}$$

$$\delta H_2(M) = -.022 \pm .011, \quad \delta L_2(M) = -.013 \pm .006. \tag{99}$$

These fits represent changes in the magnitude of station displacements due to lunar tides of characteristic size 2 cm and -1 cm for the Grasse and McDonald sites, respectively. These tidal displacements will have some synodic periodicity. This occurs directly for the solar tide because the scalar product $\hat{R}\cdot\hat{a}$ will vary as $\cos D$ (the station unit vector will point approximately toward the Moon, as best as possible, at the times of ranging measurements), while the synodic periodicity occurs indirectly for the lunar tide because the previously mentioned scalar product will diminish with synodic periodicity as observers tend to range with the Sun as low in

the sky as possible near a new moon phase. Although our fits for the Love numbers showed substantial shifts from the nominal model values, we found changes in the synodic bin-averaged post-fit residuals of no more than 1 mm over the useful range of synodic phase.

Because of the rotation of Earth and movement of the Sun and Moon, a site's actual tidal displacement consists of a superposition of a number of oscillatory motions of different frequencies. The Love numbers which represent the response of Earth to tidal forces appear to be frequency-dependent, especially in the diurnal band (frequencies clustered close to a cycle per day), and the displacement of each frequency has different dependence on the site latitude. Forcing the Love numbers to be frequency-independent is a possible explanation for the strong site-dependence of our Love number fits, this dependence then becoming a surrogate for the suppressed latitude dependence which would be a consequence of the frequency dependence. An improved dynamical Love number model should be introduced into the LLR basic model. But the existence of other site-dependent phenomena cannot yet be ruled out as reasons for the results given in Eqs. (98) and (99), and the possibility of the correlation of our site-dependent findings with similar effects in data accumulated by satellite laser and global positioning system (gps) ranging needs to be investigated.

ACKNOWLEDGMENTS

K.N. was supported by National Aeronautics and Space Administration contract NASW-97008, and he thanks Jim Williams of the Jet Propulsion Laboratory for numerous helpful discussions on the topic of this paper.

APPENDIX

Starting from initial conditions contained in the $DE200$ solar system ephemeris, the trajectories of the relevant bodies are obtained by numerical integration of the Einstein-Infeld-Hoffman relativistic N-body equations of motion as represented in isotropic, solar system barycentric coordinates. The non-spherical gravitational interactions between Earth and the Moon are included up to the fourth order spherical harmonics.

The Moon's orientation is obtained from Eulerian equations of rotational motion, modified by elasticity and energy dissipation processes in the Moon. Torques are produced by the Sun and Earth, including the latter's quadrupole moment field. The lunar librations are integrated, and the relativistic geodetic precession of the lunar spin is included.

Constants adopted for the computations are from the IAU-recommended IERS 1996 Conventions Standards [8], while Earth's rotation is described using the IAU 1980 nutation series and the values of Zhu *et al.* [9] for the 9.3 y, annual, semi-annual, and semi-monthly nutation periods. The precession angles of Lieske *et al.* [10] are employed, but the 18.6 y period coefficients and the luni-solar precession constant are determined in the multi-parameter model fit.

Earth orientation parameters are taken from a combined solution produced by R. Gross at JPL (COMB95) [17]. Tidally driven diurnal and semi-diurnal UT1 variations from Ray *et al.* [11] are added to the UT1 input file.

Tidal effects in the solid earth ($L=2$ only) on station coordinates are evaluated using the assumption of two (vertical and horizontal displacement) constant Love numbers. Ocean loading corrections are made [8], and plate tectonic motion is taken from the Nuvel NNR-1 model [12].

The general relativistic transformations between isotropic solar system barycentric coordinates and geocentric coordinates (e.g. [13]) are carried out for laser station and reflector positions. The Hirayama *et al.* [14] series is used to transform geocentric time TDT (terrestrial dynamical time) to barycentric time TDB (barycentric dynamical time).

The laser propagation times are corrected for the gravitational potentials of the Sun and Earth (Shapiro effect).

The model of Marini and Murray [15] is used to make the atmospheric corrections to the laser propagation times.

Correction of the lunar orbit (relative to Earth) due to the solar radiation pressure forces on these bodies is made using the analysis of Vokrouhlicky [16].

[1] K. Nordtvedt, Phys. Rev. **170**, 1186 (1968).
[2] K. Nordtvedt, Icarus **114**, 51 (1995).
[3] T. Damour and D. Vokrouhlicky, Phys. Rev. D **53**, 4177 (1996).
[4] J. G. Williams, X. X. Newhall, and J. O. Dickey, Phys. Rev. D **53**, 6370 (1996). They quote -0.9 cm for A_{EP} after making a 0.3 cm correction for the perturbation of the Earth-Moon system by solar radiation pressure. We use Vokrouhlicky's value [16] which is closer to 0.4 cm and adjust their number accordingly to be on the same basis with respect to this effect.
[5] J. Müller, M. Schneider, K. Nordtvedt, and D. Vokrouhlicky, in the Proceedings of the 8th Marcel Grossman Meeting, Jerusalem, 1997.
[6] J. Dickey *et al.*, Science **265**, 482 (1994).
[7] K. Nordtvedt, Phys. Rev. **169**, 1017 (1968).
[8] IERS Conventions, IERS Technical Note 21, edited by D. D. McCarthy, 1996.
[9] S. Y. Zhu, E. Groten, and C. Reigber, Astron. J. **99**, 1024 (1990).
[10] J. Lieske, T. Lederle, W. Fricke, and W. Morando, Astron. Astrophys. **58**, 1 (1977).
[11] R. D. Ray, D. J. Steinberg, B. F. Chao, and D. E. Cartwright, Science **264**, 830 (1994).
[12] IERS Standards, IERS Technical Note 13, edited D. D. McCarthy, 1992.
[13] J. Müller, Analyse von Lasermessungen zum Mond im Rhamen einer Post-Newton schen Theorie, DGK, Reihe C, No. 383, München, 1991.
[14] Th. Hirayama, H. Kinoshita, M. K. Fujimoto, and T. Fuku-

shima, in Proceedings of the IUGG General Assembly, Vancouver, Canada, 1987.

[15] J. W. Marini and C. W. Murray, "Corrections of Laser Ranging Tracking Data For Atmospheric Refraction at Elevations Above 10 Degrees," NASA Technical Report No. X-591-73-531, 1973.

[16] D. Vokrouhlicky, Icarus **126**, 293 (1997).

[17] R. S. Gross, "A combination of EOP measurements: COMB95 & POLE95," in JPL Contributions to the International Earth Rotation Service (IERS) Annual Report for 1995, JPL Geodesy and Geophysics Report No. 255, 1996 (unpublished).